Subdiffusion in Peptides Originates from the Fractal-Like Structure of Configuration Space

Thomas Neusius* and Isabella Daidone

Computational Molecular Biophysics, Interdisziplinäres Zentrum für wissenschaftliches Rechnen (IWR), Universität Heidelberg, Im Neuenheimer Feld 368, D-69120 Heidelberg, Germany

Igor M. Sokolov

Institut für Physik, Humboldt-Universität zu Berlin, Newtonstraße 15, D-12489 Berlin, Germany

Jeremy C. Smith†

Center for Molecular Biophysics, Oak Ridge National Laboratory, P.O. Box 2008, Oak Ridge, Tennessee 37831-6164, USA

(Received 18 January 2008; published 6 May 2008)

Molecular dynamics simulation of oligopeptide chains reveals configurational subdiffusion at equilibrium extending from 10^{-12} to 10^{-8} s. Trap models, involving a random walk with a distribution of waiting times, cannot account for the subdiffusion, which is found rather to arise from the fractal-like structure of the accessible configuration space.

DOI: 10.1103/PhysRevLett.100.188103 PACS numbers: 87.14.ef, 05.20.−y, 87.15.ap, 87.15.Ya

Anomalous diffusive dynamics of atoms in biological macromolecules has been the subject of considerable experimental and theoretical attention [1–10]. The distance autocorrelation functions probed in single-molecule electron transfer experiments follow a subdiffusive, Mittag-Leffler-like decay with a power-law tail decaying as $\sim t^{-0.51}$ [2] on time scales stretching from milliseconds to seconds [3,4]. Neutron scattering experiments [5] and molecular dynamics (MD) simulations [6] have provided evidence for anomalous diffusion existing also on the picosecond and nanosecond time scales.

Several theoretical models have been applied to explain the experimental and MD results. One model uses the generalized Langevin equation with a memory kernel and time correlated, ''colored'' Gaussian noise in a harmonic potential [4]. Harmonic models of proteins that are generalizations of the Rouse chain have also been applied [7]. The above harmonic models were found to predict power-law behavior, but restricted to $\sim 10^{-9}$ to 10^{-8} s time scales [8], i.e., much shorter than observed in the electron transfer experiments. An alternative to models with harmonic potentials is trapping, i.e., involving multiple minima on the energy landscape [11]. Trapping models incorporating distributions of effective escape rates have been used to interpret both the 10^{-3} to 10^{0} s time scale experimental data [3] and 10^{-12}–10^{-9} s MD data [9].

The trapping models are essentially equivalent to the continuous time random walk (CTRW) description [12], in which the random walker waits between two successive jumps for a time taken from a waiting-time distribution derived from a distribution of escape rates. CTRW in the subdiffusive case is subject to aging, meaning it is not time invariant and is a nonequilibrium, nonergodic model [12–14]. Therefore, the question arises as to the usefulness of applying CTRW (and trapping models) to equilibrium simulation and experimental data. A further question concerns the generality of the power-law kinetics, and, for example, whether the subdiffusive behavior is seen in biological systems smaller than proteins, such as peptides.

To address the above questions here MD simulations of peptides in aqueous solution are analyzed. As peptides are smaller than proteins, the simulations were able to be performed on the microsecond time scale, i.e., a time scale in which the dynamical quantities of interest have converged, and over more than 2 orders of magnitude longer than previous MD analyses of subdiffusion. The model systems are $(GS)_nW$ peptides (where G = glycine, S = serine, and W = tryptophan, $n = 2$, 3, 5, and 7) with simulation lengths of 0.8, 1.0, 1.9, and 2.5 μs, respectively. The simulation protocol is described in [15]. The MD simulation data used were generated with the GROMACS software package and the GROMOS96 force field [16], in the NVT ensemble at 293 K with isokinetic temperature coupling [17] to maintain constant temperature. For the analysis translation and rotation were subtracted by fitting to a reference structure. Similar results to those described here were obtained by applying the present analysis to a β-hairpin peptide in both explicit and implicit water (results not shown).

The simulation provides a set of the atomic trajectories in the full configuration space of the peptide, and thus furnishes, in principle, complete dynamical information. It has been shown that, to simplify interpretation, the essential dynamics of biomolecules can be reduced to low-dimensional subspaces via principal component analysis (PCA) [18]. PCA involves the diagonalization of the symmetric atomic fluctuation covariance matrix C, the elements of which are $c_{ij} = \langle \Delta x_i(t) \Delta x_j(t) \rangle$, where $\Delta x_i(t) = x_i(t) - \bar{x}_i$ is the deviation from the mean position $\bar{x}_i$.

The diagonalization leads to a new set of coordinates. The eigenvalues give the contribution to the mean squared

displacement (MSD). Lower PCs, i.e., with high eigenvalues, contain most of the diffusive dynamics [18,19]. With decreasing eigenvalues the principal modes exhibit lower variances and the shapes of the potentials of mean force tend to be closer to harmonic [9,19].

For harmonic systems consisting of subunits of equal mass the PCs correspond to the normal modes. In the case of the $(GS)_nW$ peptides, and as is commonly observed for proteins at physiological temperatures [18,20], the low modes were found to be delocalized over the peptide with strongly anharmonic potentials of mean force (results not shown). This suggests that harmonic models are inappropriate for the description of the low PC dynamics. The probability density functions for the lowest PCs were found to contain a statistical error of ≈ 1 kT, whereas the higher modes are converged. The statistical error was found to not influence the results presented here.

The potentials of mean force of the first and the second halves of the simulations coincide with statistical errors in the range of ≈ 1 kT, and the trajectory can thus be considered as in equilibrium.

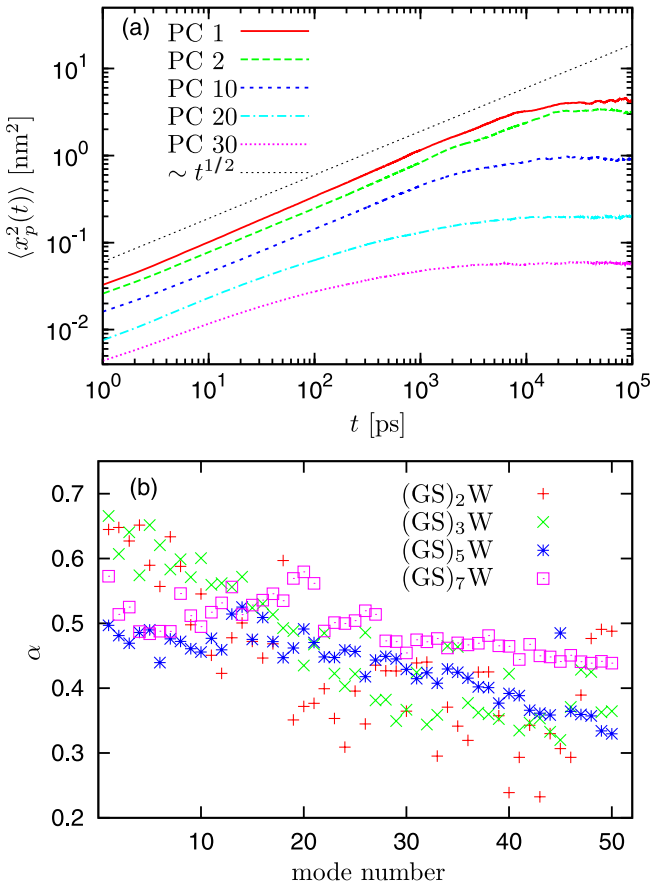

FIG. 1 (color online). (a) MSD for different PCs of $(GS)_5W$. (b) Mean squared displacement exponents α for the four peptides as a function of mode number, obtained by fitting a linear function of log$t$ to log$\langle x(t)^2\rangle$ in the t range 1 to 10 ps using a least-squares method. Error bars are smaller than symbol size.

The quantity that provides the most direct access to subdiffusivity is the MSD of the coordinate $x_p(t)$ corresponding to PC p. For a single MD trajectory $\langle x_p^2(t)\rangle$ is calculated by time averaging, i.e., for a discrete trajectory with N frames

$$\langle x_p^2(t)\rangle := \frac{1}{N-t}\sum_{\tau=0}^{N-t}[x_p(t+\tau)-x_p(\tau)]^2.$$

For the lower PCs the MSD follows a strongly subdiffusive pattern $\langle x_p^2(\tau)\rangle \propto \tau^\alpha$ extending for the lowest PCs over four decades (10^{-12}–10^{-8} s) until eventually saturating [Fig. 1(a)]. To compare the exponents on the time scale 1–10 ps linear fits were performed to log$\langle x_p^2(\tau)\rangle$ vs log$t$ for each mode [Fig. 1(b)]. The values of α are <1 for all peptide lengths. The tendency of the exponents to decrease with the mode number may be related to increased harmonicity of the higher modes. The decrease is stronger for the shorter peptides, indicative of fewer delocalized modes.

The asymptotic behavior of the waiting-time distribution was obtained by mapping the dynamics along the principal coordinates onto a two-state process (Fig. 2). The results show a power-law behavior, $w(t) \sim t^{-1-\beta}$, again extending to the 10 ns range. The exponent β lies in the range of 0.5 to 0.6 for the lowest modes.

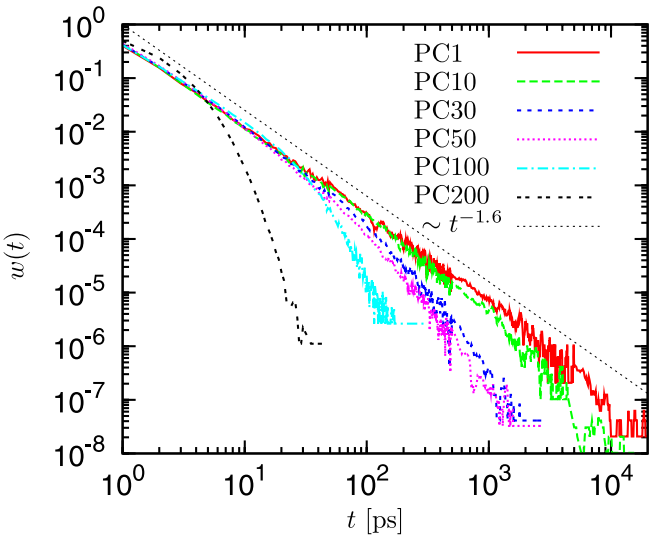

FIG. 2 (color online). Waiting-time distribution for different PCs of $(GS)_5W$ obtained by projecting time series of each PC onto a two-state space. For PCs with multiminimum potentials of mean force, i.e., the lowest, the two states were defined by dividing the x space into the two parts either side of the position of the highest barrier in the potential of the mean force. For the higher PCs, which have only a single minimum, by symmetry the space was divided at the position of the minimum. The results were found to be independent of the precise location of the partition. In order to improve statistics at long times, the data were piecewise convoluted with filters of different sizes.

We now examine whether CTRW can be applied to analyze the PC dynamics. Provided $w(\tau)$ has a power-law tail, $\sim\tau^{-1-\beta}$ with $\beta < 1$, and provided that at $t = 0$ the structure undergoes a jump, then in CTRW the mean number of jumps taken up to time t follows the power law $\langle N(t)\rangle \propto t^{\beta}$, where the mean is an ensemble average, i.e., over different series of waiting times taken from $w(\tau)$. It can then be shown that the longer the walker moves, i.e., the more traps are inspected, the higher the probability is of finding a very deep trap and staying there for a relatively long time [14]. The MSD in CTRW is proportional to the number of jumps, so the MSD during the interval $[t, t+\tau]$ varies as $\langle x^2(\tau)\rangle \propto \langle N(t+\tau)\rangle - \langle N(t)\rangle \propto (t+\tau)^{\beta} - t^{\beta}$ [14]. The dependence of $\langle x^2(\tau)\rangle$ on t for all $\beta < 1$ corresponds to aging. For $t \gg \tau$ normal diffusive behavior, $\langle x^2(\tau)\rangle \propto t^{\beta-1}\tau$, is seen. For larger $\tau \gg t$ the MSD will be subdiffusive, i.e., $\langle x^2(\tau)\rangle \sim \tau^{\beta}$ [12].

To illustrate the aging effect, Fig. 3 shows $\langle x^2(t)\rangle$ calculated with $\beta = 0.5$ in two ways, as an ensemble average over 10 000 CTRW trajectories and as a time average. For the ensemble average, initially $\langle x^2(t)\rangle \propto t$ crossing over to $\langle x^2(t)\rangle \propto \sqrt{t}$. In contrast, the time averaged MSD has a ballistic, t^2 behavior for small t, and the long-time behavior is linear in t.

The above discussion shows that the subdiffusion in CTRW is an aging effect, requiring dependence on the initial condition. Time averaging in CTRW removes the initial condition dependence, and thus the subdiffusivity.

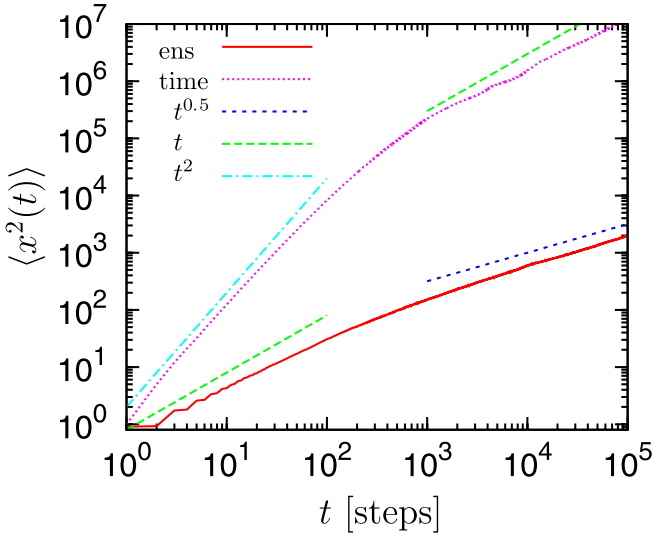

FIG. 3 (color online). Normalized MSD of a CTRW with $\beta = 0.5$. The waiting times t_w were generated from a uniform random variable $r \in [0, 1]$ using the transformation $t_w = r^{-1/\beta} - 1$. Jump lengths were taken from a normal distribution. The red line ("ens") shows $\langle x^2(t)\rangle$ calculated as an ensemble average over 10 000 realizations of a CTRW. $\langle x^2(t)\rangle$ calculated as a time averaged quantity is given in magenta ("time"). The blue and green lines (dashed: see legend) give the asymptotic power-law behavior and serve to guide the eye.

The MSD calculated from the MD simulation in Fig. 1(a) is the outcome of time averaging. Therefore, CTRW cannot explain subdiffusion in the MD MSD.

CTRW is equivalent to a trap model consisting of a random walk between minima with a distribution of waiting times. It is insufficient to explain subdiffusion at equilibrium. Rather, subdiffusion at equilibrium arises from the geometric and kinetic relationships between the regions visited on the energy landscape. These relationships can be obtained via discretization with a transition network [21,22], in which the nodes correspond to regions in the configuration space and the edges are weighted proportional to the rates of transitions between the regions. Here, we compute the weighted transition network corresponding to the subset of diffusive modes in the simulation and examine the topology of the network. To calculate the transition network 10 000 points in the subspace of the ten lowest PCs were randomly chosen, and are denoted by $\{\mathbf{r}(i)|i = 1, \ldots, 10\,000\}$. A discretized trajectory was generated by replacing each MD coordinate frame with the number of the point that lies closest in the ten-dimensional subspace, hence defining the regions.

From the discretized trajectory a transition matrix $R(\Delta t)$ can be calculated with the elements

$$r_{ij}(\Delta t) = \frac{\sum_t \delta[x(t) - j]\delta[x(t+\Delta t) - i]}{\sum_t \delta[x(t) - j]},$$

$\delta[x]$ being the Dirac delta function, t the discrete time, Δt a multiple of the discrete time step of the trajectory, and $x(t)$ the space-discretized trajectory. The elements $r_{ij}(\Delta t)$ give the relative probability of being at node i at time $t + \Delta t$, given that the system is at node j at time t. The matrix depends on Δt. If Δt is assumed to be sufficiently large that any memory effects arising from the degrees of freedom not explicitly included are small, then the discrete dynamical trajectory $\kappa(t)$, $t = 1, \ldots, n$ can be calculated such that the occupation vector $\mathbf{p} = (p_\kappa)_\kappa$ obeys $\mathbf{p}(t + \Delta t) = R(\Delta t)\mathbf{p}(t)$. If the geometrical structures in configuration space are crucial for the subdiffusive behavior, then the MSD in the configuration space,

$$\langle \mathbf{x}^2(t)\rangle = \frac{1}{n-t}\sum_{\tau=0}^{n-t}[\mathbf{r}(\kappa(t+\tau)) - \mathbf{r}(\kappa(\tau))]^2,$$

must also be subdiffusive.

In Fig. 4 $\langle x^2(t)\rangle$, calculated for PC 1 on the basis of transition matrices on different time scales, Δt, is compared with the corresponding MSD from the MD trajectory. On all time scales subdiffusive behavior is seen. For the shorter time scales ($\Delta t = 1$ and 10 ps) the slopes differ from the all-atom MD, due probably to non-Markovian effects. However, on the 100 and 1000 ps time scales the agreement is good. The same behavior is found for each of the ten lowest PCs (results not shown). Changing the transition matrix in such a way that all allowed transitions are equally likely did not significantly affect the subdiffu-

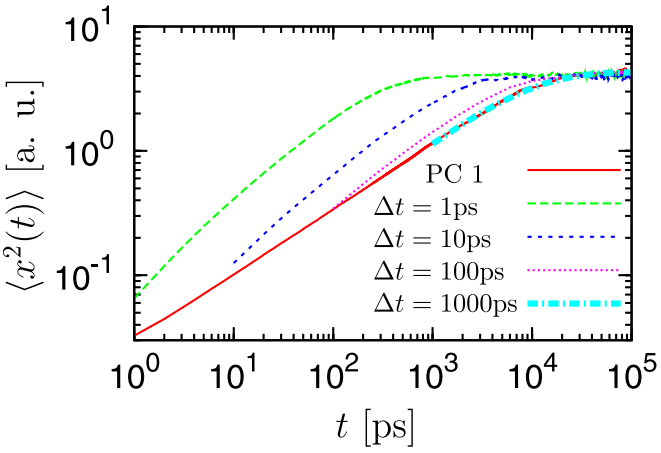

FIG. 4 (color online). MSD of trajectories generated from the transition matrix $R(\Delta t)$ for different Δt together with the corresponding MSD from the original trajectory. The matrix $R(\Delta t)$ was derived from the $(GS)_5W$ trajectory in the subspace of the first ten PCs.

sion properties, thus emphasizing the importance of the geometry of the configuration space.

The subdiffusion found in the generated data demonstrates the importance of the geometrical properties of the accessible volume in the configuration space. The presence of subdiffusion on a transition network indicates that the network behaves as a fractal. The fractal dimension d_f characterizes the scaling of the mass of a fractal with the linear distance, $M \sim R^{d_f}$ [23]. A power-law fit to the mass scaling leads to $d_f = 5.5$, 6.0, 6.5, and 8.5 for $\Delta t = 1$ ps, 10 ps, 100 ps, and 1 ns, respectively. From the probability of finding a random walker at time t at the origin, $P(t) \sim t^{-d_s/2}$, the corresponding spectral dimension follows as $d_s = 2.8$, 2.8, 2.4, and 2.4 and the exponent of the MSD α for a random walk on the transition networks is $\alpha = 0.7$, 0.7, 0.6, and 0.45. The discrepancy between d_f and d_s/α of $\approx 50\%$ is likely to arise from the finite size of the transition network.

The present analysis of the behavior of PCs in MD simulations of $(GS)_nW$ peptides in aqueous solution shows that the relaxation in the low PCs is subdiffusive, displaying power-law behavior over four decades in the time domain. The behavior observed cannot be explained with simple trap models, since it is not due to aging. Instead, the fractal-like structure of the accessible volume in configuration space is responsible for the subdiffusivity. This structure is well represented using a transition matrix approach. Future research is warranted into the degree of generality of the present conclusions in biopolymer physics.

I. M. S. thankfully acknowledges financial support by DFG within the No. SFB555 research program. We thank Professor G. R. Kneller for useful discussions.

*To whom correspondence should be addressed.
thomas.neusius@iwr.uni-heidelberg.de
†Also at IWR, Universität Heidelberg, Heidelberg, Germany.

[1] W. G. Glöckle and T. F. Nonnenmacher, Biophys. J. **68**, 46 (1995).
[2] W. Min *et al.*, Phys. Rev. Lett. **94**, 198302 (2005).
[3] H. Yang *et al.*, Science **302**, 262 (2003).
[4] S. C. Kou and X. S. Xie, Phys. Rev. Lett. **93**, 180603 (2004).
[5] G. R. Kneller, Phys. Chem. Chem. Phys. **7**, 2641 (2005).
[6] G. R. Kneller and K. Hinsen, J. Chem. Phys. **121**, 10278 (2004).
[7] R. Granek and J. Klafter, Phys. Rev. Lett. **95**, 098106 (2005).
[8] J. Tang and S.-H. Lin, Phys. Rev. E **73**, 061108 (2006).
[9] G. Luo *et al.*, J. Phys. Chem. B **110**, 9363 (2006).
[10] Y. Matsunaga, C.-B. Li, and T. Komatsuzaki, Phys. Rev. Lett. **99**, 238103 (2007).
[11] C. Monthus and J.-P. Bouchaud, J. Phys. A **29**, 3847 (1996).
[12] R. Metzler and J. Klafter, Phys. Rep. **339**, 1 (2000).
[13] E. Barkai and Y.-C. Cheng, J. Chem. Phys. **118**, 6167 (2003); J. W. Haus and K. W. Kehr, Phys. Rep. **150**, 263 (1987).
[14] I. M. Sokolov, A. Blumen, and J. Klafter, Physica (Amsterdam) **302A**, 268 (2001); I. M. Sokolov, A. Blumen, and J. Klafter, Europhys. Lett. **56**, 175 (2001).
[15] I. Daidone *et al.*, Proc. Natl. Acad. Sci. U.S.A. **104**, 15230 (2007); I. Daidone *et al.*, J. Am. Chem. Soc. **127**, 14825 (2005).
[16] H. J. C. Berendsen, D. van der Spoel, and R. van Drunen, Comput. Phys. Commun. **91**, 43 (1995).
[17] D. Brown and J. H. R. Clarke, Mol. Phys. **51**, 1243 (1984).
[18] A. Amadei, A. B. M. Linssen, and H. J. C. Berendsen, Proteins **17**, 412 (1993).
[19] A. L. Tournier and J. C. Smith, Phys. Rev. Lett. **91**, 208106 (2003).
[20] H. J. C. Berendsen, J. R. Grigera, and T. P. Straatsma, J. Phys. Chem. **91**, 6269 (1987).
[21] F. Noé *et al.*, J. Chem. Phys. **126**, 155102 (2007); F. Noé *et al.*, J. Chem. Theory Comput. **2**, 840 (2006).
[22] D. Gfeller *et al.*, Phys. Rev. E **76**, 026113 (2007); J. P. K. Doye, Phys. Rev. Lett. **88**, 238701 (2002); A. Scala, L. A. Nunes Amaral, and M. Barthélémy, Europhys. Lett. **55**, 594 (2001).
[23] S. Havlin and D. Ben-Avraham, Adv. Phys. **36**, 695 (1987).